DOI 10.24425/aee.2023.146051

Research on improving low-frequency oscillation characteristics of wind power grid-connected power system with doubly-fed wind generator based on virtual impedance power system stabilizer

PING HE[1] ✉, YONGLIANG ZHU[2], QIUYAN LI[3], JIALE FAN[1], YUKUN TAO[1]

[1] *Zhengzhou University of Light Industry, College of Electrical and Information Engineering China*

[2] *Zhengzhou University of Light Industry, College of Materials and Chemical Engineering China*

[3] *State Grid Henan Electric Power Company, Economic and Technical Research Institute China*

e-mail: ✉*hplkz@126.com*

(Received: 18.01.2023, revised: 17.06.2023)

Abstract: The grid integration of large-scale wind power will alter the dynamic characteristics of the original system and the power distribution among synchronous machines. Meanwhile, the interaction between wind turbines and synchronous machines will affect the damping oscillation characteristics of the system. The additional damping control of traditional synchronous generators provides an important means for wind turbines to enhance the damping characteristics of the system. To improve the low frequency oscillation characteristics of wind power grid-connected power systems, this paper adds a parallel virtual impedance link to the traditional damping controller and designs a DFIG-PSS-VI controller. In the designed controller, the turbine active power difference is chosen as the input signal based on residual analysis, and the output signal is fed back to the reactive power control loop to obtain the rotor voltage quadrature component. With DigSILENT/PowerFactory, the influence of the controller parameters is analyzed. In addition, based on different tie-line transmission powers, the impact of the controller on the low-frequency oscillation characteristics of the power system is examined through utilizing the characteristic root and time domain simulation analysis.

Key words: doubly-fed induction wind turbine, grid-connected wind power, low-frequency oscillation, power system stabilizer, virtual impedance

1. Introduction

At the Climate Ambition Summit, China proposed a target of achieving over 1.2 billion kilowatts of combined wind and solar energy capacity by 2030, representing an increase of nearly threefold from current levels. The problem of low-frequency oscillations in wind power generated by large-scale doubly-fed induction generators (DFIGs) is gaining increasing attention due to the rapid development of wind power [1]. Numerous scholars now acknowledge that as the size of the power grid expands, its ability to dampen oscillations weakens. As a result, the growing number of DFIGs connected to the grid necessitates enhancing the damping capabilities of the system and effectively suppressing low-frequency oscillations [2–5].

During instances of power system disturbances, low-frequency power system oscillations arise, when the negative damping component of the automatic voltage regulator of the generator exceeds the inherent positive damping component of the generator [6]. In the recently published works, the methods for analyzing low-frequency oscillations can be mainly divided into two categories, one is to analyze by building a mathematical model of the power system, and the other is to analyze based on the actual measured signals of the power system. Among them, the damped torque analysis method and the eigenvalue analysis method are the analysis methods based on linear theory; the time domain simulation method and the signal analysis method are the analysis methods based on nonlinear theory [7–9]. The article uses a combination of two methods to analyze the low-frequency oscillation patterns of the system. The feasibility of the method is greatly improved.

A decline in damping is occurring in power systems due to the increasing proportion of power electronics in new power systems, and at this time the system can exhibit negative damping for low-frequency oscillations, which can worsen the power system. The use of power system stabilizers (PSS) to increase system damping and thus suppress low-frequency oscillations is a common method in conventional power systems [10–13]. Reference [14] elucidates the effect of wind power on small disturbance stability and introduces control methods for wind turbines to suppress internal and power system oscillation modes. Reference [15] presents fast active power control techniques for variable speed wind turbines and discusses their applicability in frequency regulation and oscillation damping in the Eastern U.S. interconnected system. Reference [16] adds control signals to the active power control link to improve the small disturbance stability of the system by regulating the DFIG active power output. References [17–19] show that damping analysis of DFIG active control may lead to shaft system oscillations, so the paper adds the control signal to the reactive control loop for regulation. Reference [20] applies the regional pole configuration method to design the parameters of power system controller (DFIG-PSS). Reference [21] establishes the state equation of the system containing DFIG-PSS, introduces the characteristic root increment into the transfer function increment iterative operation, and compares the parameter sensitivity and transfer function sensitivity error and the control effect of the corresponding designed DFIG-PSS by simulation. Reference [22] clarifies that DFIG can significantly enhance wind farm damping to the grid while maintaining the quality of voltage control by incorporating a suitable DFIG-PSS.

At present, a large amount of references has been conducted for the design of DFIG-PSS, but little references have considered the interference of the equivalent output impedance of PSS to the system. Based on this background, the use of virtual impedance (VI) is considered to correct the

intrinsic output impedance of PSS to give the conventional PSS better output characteristics and thus more effective suppression of low frequency oscillations in power systems. In reference [23], a virtual synchronous generator (VSG) with pre-synchronization control approach is employed for DFIG, and virtual impedance is introduced in the reactive power control loop to replace the reference input with virtual current to achieve a fast and effective smooth grid integration of doubly-fed wind turbines. In reference [24], the mechanism of the effect of VSG control approach on small disturbance stability was elucidated, and the system's small disturbance stability can be improved by increasing appropriately the inductance of the virtual impedance link.

Although the conventional power system stabilizer (PSS) plays a vital role in suppressing low frequency oscillations, its output impedance is non-resistive in nature. Based on this, we propose that adding virtual impedance to the conventional PSS can be used to adjust the output impedance characteristics of the conventional PSS, enhance the damping characteristics of the power system, and suppress low frequency oscillations in the power system more effectively. The proposed PSS-VI adds a virtual impedance link to the conventional PSS and uses a closed-loop negative feedback control method to enhance the controller's immunity to interference. Considering that the DFIG active control loop with a controller may cause the rotor shaft system oscillation problem, the control signal is added to the DFIG rotor side converter (RSC) reactive control link in this paper. The active power difference is selected as the PSS-VI control input signal, and the controller is added to the DFIG rotor-side control reactive power control link. Finally, the PSS-VI model is created utilizing DigSILENT/PowerFactory simulation software., and the simulation is verified on a 4-machine 2-area system.

2. Introduction of power system stabilizer control

2.1. Conventional PSS

The PSS is an auxiliary controller used in a wide range of excitation control systems. By providing an auxiliary control signal for the excitation system, the generator generates an electromagnetic torque component that is synchronized with the rotor's angular velocity deviation, which in turn increases system damping and suppresses power system's low-frequency oscillations.

The traditional PSS structure block diagram is shown in Fig. 1 [25].

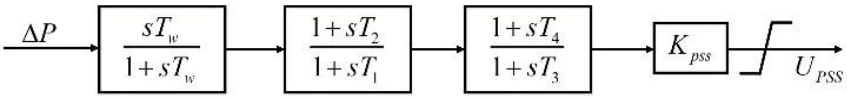

Fig. 1. Traditional PSS structure block diagram

The PSS transfer function is as Eq. (1),

$$G(s) = K_{\mathrm{PSS}} \frac{sT_W(1+sT_2)(1+sT_4)}{(1+sT_W)(1+sT_1)(1+sT_3)}, \tag{1}$$

where the shuffle link's time constant is T_W, T_1, T_2, T_3 and T_4 are the constants of time in the overrun lag link, and K_{PSS} is the PSS gain.

2.2. DFIG-PSS principle of low frequency oscillation suppression

In the rotor magnetic chain of the DFIG, the d–q components are as follows:

$$\begin{aligned} \Psi_{dr} &= L_{rr} i_{dr} - L_m i_{ds} \,, \\ \Psi_{qr} &= L_{rr} i_{qr} - L_m i_{qs} \,, \\ L_{rr} &= L_r + L_m \,, \end{aligned} \tag{2}$$

where $\Psi_{dr}, \Psi_{qr}, i_{ds}, i_{qs}, i_{dr}, i_{qr}$ are the d-q-axis components of the rotor flux, the stator current and the rotor current, respectively. L_m represents the mutual inductance between the stator and rotor, and L_r symbolizes the rotor self-inductance.

The expressions for the rotor current and the d–q component of the rotor voltage can be derived from Eq. (2) as follows:

$$\begin{aligned} i_{dr} &= \frac{\Psi_{dr} + L_m i_{ds}}{L_{rr}} \,, \\ i_{qr} &= \frac{\Psi_{qr} + L_m i_{qs}}{L_{rr}} \,, \\ u_{dr} &= r_r i_{dr} - s\omega_s \Psi_{qr} + \frac{1}{\omega_b} \frac{\mathrm{d}\Psi_{dr}}{\mathrm{d}t} \,, \\ u_{dr} &= r_r i_{dr} - s\omega_s \Psi_{qr} + \frac{1}{\omega_b} \frac{\mathrm{d}\Psi_{dr}}{\mathrm{d}t} \,, \\ u_{qr} &= r_r i_{qr} - s\omega_s \Psi_{dr} + \frac{1}{\omega_b} \frac{\mathrm{d}\Psi_{qr}}{\mathrm{d}t} \,, \end{aligned} \tag{3}$$

where: u_{dr}, u_{qr} are the rotor voltage d-axis and q-axis components, ω_s is the synchronous speed, ω_b is the speed reference value, r_r is the rotor resistance and s is the rotation difference. From Eq. (3), it is obtained that:

$$\begin{aligned} u_{dr} &= r_r \frac{\Psi_{dr} + L_m i_{ds}}{L_{rr}} - s\omega_s \Psi_{qr} + \frac{1}{\omega_b} \frac{\mathrm{d}\Psi_{dr}}{\mathrm{d}t} \,, \\ u_{qr} &= r_r \frac{\Psi_{qr} + L_m i_{qs}}{L_{rr}} - s\omega_s \Psi_{dr} + \frac{1}{\omega_b} \frac{\mathrm{d}\Psi_{qr}}{\mathrm{d}t} \,. \end{aligned} \tag{4}$$

The d-q component of the potential after the transient reactance is defined as:

$$\begin{aligned} e_d &= -\frac{\omega_s L_m}{L_{rr}} \Psi_{qr} \,, \\ e_q &= -\frac{\omega_s L_m}{L_{rr}} \Psi_{dr} \,, \end{aligned} \tag{5}$$

where e_d, e_q correspond to the d and q-axis potential components after the transient reactance, respectively.

Combining Eqs. (4) and (5), the derivative of the potential after the transient reactance can be obtained as Eq. (6).

$$\begin{aligned} \frac{\mathrm{d}e_d}{\mathrm{d}t} &= -\frac{\omega_b}{T_0} \left[e_d - (X - X')i_{qs} \right] + s\omega_s e_q - \frac{\omega_s L_m}{L_{rr}} u_{qr} \,, \\ \frac{\mathrm{d}e_q}{\mathrm{d}t} &= -\frac{\omega_b}{T_0} \left[e_q - (X - X')i_{ds} \right] + s\omega_s e_d + \frac{\omega_s L_m}{L_{rr}} u_{dr} \,, \end{aligned} \tag{6}$$

where: L_s is the stator leakage inductance, $X = \omega_s L_{ss} = \omega_s(L_s + L_m)$ is the open circuit reactance, X' is the DFIG transient reactance, and $T_0 = \dfrac{L_{rr}}{r_r} = \dfrac{L_r + L_m}{r_r}$ is the transient open circuit time constant. According to Eq. (6), the vector differential equation of the potential inside DFIG can be written as Eq. (7):

$$\frac{\mathrm{d}E_g}{\mathrm{d}t} = -\frac{\omega_b}{T_0}\left[E_g - j(X - X')I_s\right] + js\omega_s E_g - j\frac{\omega_s L_m}{L_{rr}}U_r\,, \tag{7}$$

where: $E_g = e_d + je_q$, $I_s = i_{ds} + ji_{qs}$, $U_s = u_{dr} + ju_{qr}$. Considering $\omega_b = 1$, Eq. (7) can be written as follows:

$$\frac{\mathrm{d}E_g}{\mathrm{d}t} = -\frac{1}{T_0}\left[E_g - j(X - X')I_s\right] + js\omega_s E_g - j\frac{\omega_s L_m}{L_{rr}}U_r\,. \tag{8}$$

In Eq. (8), E_g is the potential inside the generator after the transient reactance, and its amplitude is determined by the rotor magnetic chain amplitude, which can be controlled by adjusting the rotor voltage U_r. It can be concluded that a change in the rotor voltage U_r caused a change in the generator internal potential E_g, which is generated in the stator, and this affects the voltage and output power of DFIG. It is assumed that E_g changes correspondingly very rapidly for U_r, so that:

$$E_g \approx \frac{L_m}{sL_{rr}}U_r\,. \tag{9}$$

Assuming that a change in the phase angle δ_r of the rotor voltage U_r will instantaneously change the phase angle δ_g of the potential E_g after the transient reactance, neglecting the power control loop effect, δ_g can be approximately equal to δ_r. The change of output power in generator, due to the action of the controller is:

$$P_{ea} = \frac{E_g E_2}{X'}\sin(\delta_g - \delta_2), \tag{10}$$

where δ_2 represents the phase angle of the generator voltage with respect to the voltage at the access bus and Eq. (10) can be linearized as:

$$\Delta P_{ea} = \frac{E_g E_2}{X'}\cos(\delta_{g0} - \delta_{20})(\Delta\delta_g - \Delta\delta_2) = K_g(\Delta\delta_g - \Delta\delta_2). \tag{11}$$

The power change caused by the change in turndown rate is that:

$$\Delta P_{eb} = K_s(\Delta\omega_s - \Delta\omega_r), \tag{12}$$

where:

$$\begin{aligned} \Delta\omega_{2s} &= \frac{s}{2\pi f}\Delta\delta_2\,, \\ \Delta\omega_{2r} &= \frac{1}{2H_2 s}\Delta P_{e2}\,. \end{aligned} \tag{13}$$

The amount of total power change is:

$$\Delta P_{e2} = \Delta P_{ea} + \Delta P_{eb}\,. \tag{14}$$

When the system oscillates, the DFIG contributes a power component to the synchronous machine. This component is in phase with the rotor speed oscillation of this generator. In order to achieve this, it is necessary to make the phase component of the power change of the DFIG opposite to the phase of the rotor speed change of the synchronous generator. Therefore, the generator damping is improved and the power and phase angle are schematically shown in Fig. 2.

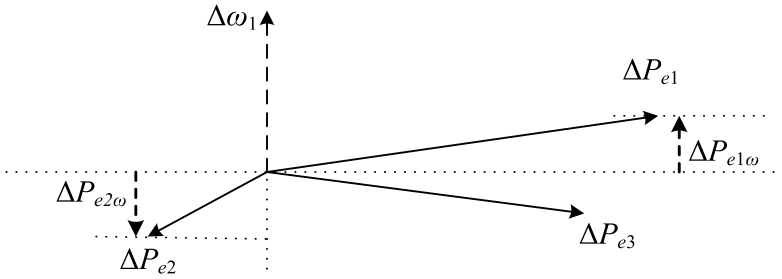

Fig. 2. Vector diagram illustrating the effect of DFIG damping power

In Fig. 2, ΔP_{ei} indicates the power delivered by the generator through the i-th bus.

The hysteresis link contained in the DFIG control loop ensures that the DFIG has a positive damping effect. According to the damping torque analysis method, assuming that the PSS is used to amplify the power vector ΔP_{e2} and rotate it counterclockwise, the DFIG damping effect on the system increases. The component of the power vector $\Delta P_{e2\omega}$ along the negative imaginary axis increases. This causes the component of the synchronous generator power vector $\Delta P_{e1\omega}$ along the positive imaginary axis to increase as well. From the synchronous generator's point of view, the power component representing the same phase of the rotor speed oscillation increases, and thus the damped power increases.

2.3. Virtual impedance-based PSS

In order to improve the stability of the power system during instances of small disturbances, this section exhibits a scheme by introducing a parallel virtual impedance link to the traditional PSS utilized in DFIGs.

A controller's parameters have a significant impact on the output impedance and system stability and response rapidity. Nevertheless, if both are considered simultaneously for the virtual impedance link parameter design, the candidate adjustment range for the controller parameters becomes smaller. By offering a virtual impedance link in the PSS control loop, this paper uses virtual impedance-based voltage control. The virtual impedance link is connected in parallel with the overrunning hysteresis link to adjust the PSS input and output. First, a suitable virtual impedance Z_{vi} is selected, and then the equivalent output impedance Z_i of PSS-VI is formed with the conventional PSS equivalent output impedance Z_{oi}, and then the impedance properties of PSS are changed to improve power system stability. As seen in Fig. 3, when the virtual impedance Z_{vi} is changed, the phase angle of Z_i will change accordingly.

Z_i is adjusted by altering the virtual impedance mode value, while ensuring the controller has a satisfactory unit step response. The schematic diagram of PSS-VI is presented in Fig. 4.

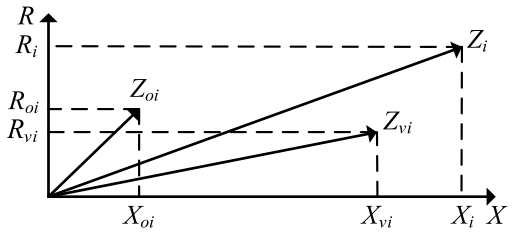

Fig. 3. Vector representation of virtual impedance

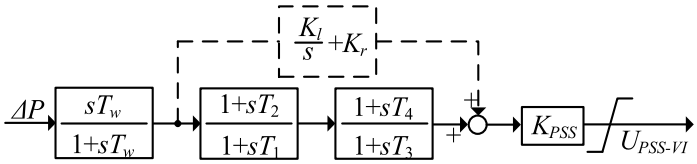

Fig. 4. PSS-VI

The various input signals have a significant impact on the PSS-VI controller's effectiveness. The input signal to the controller can be selected from rotor speed, voltage, current or frequency, voltage, current or frequency, typically based on residual analysis method. The difference between the active power reference value P_s^* of the DFIG and the active power measurement P_s is chosen here as the input signal. The output signal $U_{\mathrm{PSS-VI}}$ is added to the reactive power control loop. The virtual impedance link uses the signal after the filtering link as input, which can ensure that the virtual impedance link is not influenced by spurious waves in the PSS input signal. The PSS-VI transfer function is represented by Eq. (15),

$$G_1(s) = K_{\mathrm{PSS}} \frac{T_W}{1+sT_W} \left(\frac{(1+sT_2)(1+sT_4)}{(1+sT_1)(1+sT_3)} + K_r + \frac{K_I}{s} \right), \tag{15}$$

where K_I and K_r are the virtual impedance link parameters and K_{PSS} is the PSS-VI controller gain.

The controller output signal is obtained from Eq. (1) and Eq. (15).

$$\begin{cases} U_{\text{PSS-VI}} = \Delta P K_{\mathrm{PSS}} \dfrac{T_W}{1+sT_W} \left(\dfrac{(1+sT_2)(1+sT_4)}{(1+sT_1)(1+sT_3)} + K_r + \dfrac{K_I}{s} \right) \\ U_{\mathrm{PSS}} = \Delta P K_{\mathrm{PSS}} \dfrac{sT_W (1+sT_2)(1+sT_4)}{(1+sT_W)(1+sT_1)(1+sT_3)} \end{cases}. \tag{16}$$

According to Eq. (16), the controller output can be organized into impedance form as shown in Eq. (17).

$$\begin{cases} U_{\text{PSS-VI}} = IZ_{oi} + IZ_{vi} \\ U_{\mathrm{PSS}} = IZ_{oi} \end{cases}, \tag{17}$$

where

$$I = \Delta P K_{\mathrm{PSS}} \frac{T_W}{1+sT_W}, \quad Z_{oi} = \frac{(1+sT_1)(1+sT_3)}{(1+sT_2)(1+sT_4)}, \quad Z_{vi} = K_r + \frac{K_I}{s}. \tag{18}$$

In Eq. (18), I is the controller equivalent current, Z_{oi} is the equivalent impedance of the conventional PSS controller, and Z_{vi} is the selected suitable virtual impedance.

According to Eq. (17), it can be seen that the introduction of parallel virtual impedance in the overrunning hysteresis link of the conventional PSS can regulate the equivalent output impedance property of the conventional PSS. The output signal $U_{\text{PSS-VI}}$ of the PSS-VI controller is made to be added to the reactive power control link, which in turn regulates the phase angle of the rotor voltage for the purpose of improving the system damping and enhancing the system stability.

3. DFIG-PSS-VI control design

3.1. DFIG-PSS-VI Implementation

The vector control approach is used to decouple the active and reactive power in the doubly-fed generator, taking into account the maximum wind power and compensating for the reactive power, as illustrated in Fig. 5. This approach uses a traditional nested loop structure, i.e., external

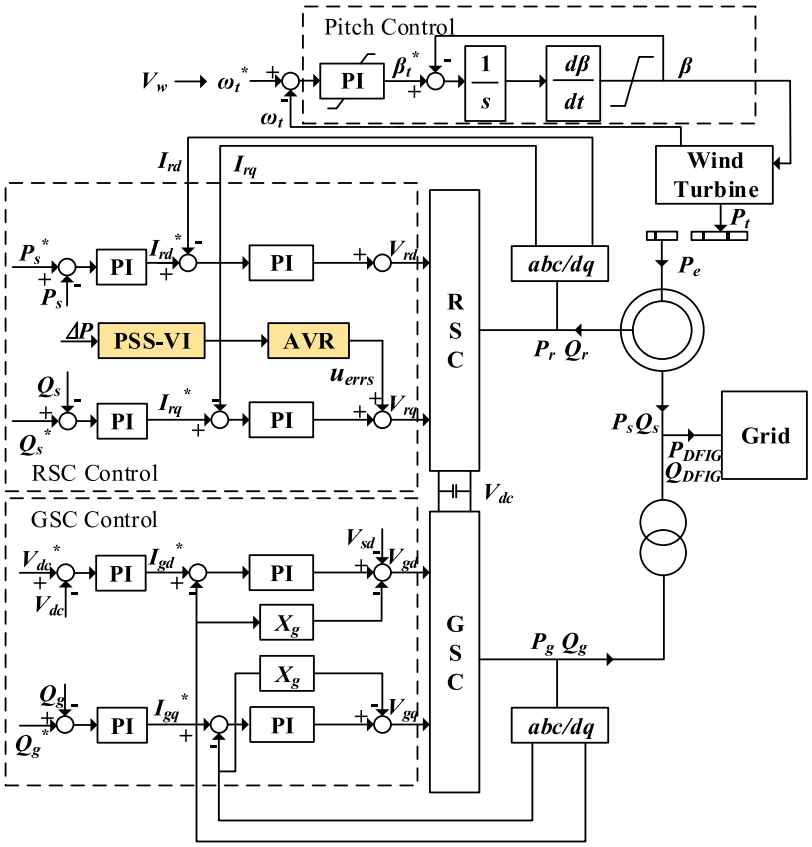

Fig. 5. DFIG-PSS-VI control structure

speed/active and reactive power and internal d-q rotor current control loops, which allows the rotor d-q reference current to be effectively estimated from the actual reference and reactive reference values, eliminating the need for a power loop controller with a nested control structure. The damping effect of a DFIG with basic power and voltage control loops on the electromechanical oscillation mode of the grid is small. However, it can be significantly enhanced by additional damping controls. The additional damping control signal is delivered to the DFIG active power or reactive power control loop by an automatic voltage regulator (AVR).

It is shown that active regulation is more effective in altering the generator electromagnetic torque. However, such regulation may compromise the DFIG shaft dynamics, while reactive regulation could impair stator voltage dynamics. In some cases, the DFIG must sacrifice a portion of its own dynamics for damping control. Therefore, both damping control and system dynamics should be taken into account during practical implementation. The UPSS-VI output control signal of PSS-VI is transmitted to the reactive power control loop and added up to derive the orthogonal components of rotor voltage.

DFIG rotor-side converter adopts the stator magnetic chain directional vector control technique, and the relationship between rotor current and RSC output voltage is

$$\begin{cases} V_{rd} = \left[\left(P_s^* - P_s\right)\left(K_{p1} + \dfrac{K_{i1}}{s}\right) - i_{rd}\right]\left(K_{p3} + \dfrac{K_{i3}}{s}\right) \\ \qquad - I_{sq} s\omega_s L_m - I_{rq} s\omega_s L_{rr} \\ V_{rq} = \left[\left(Q_s^* - Q_s\right)\left(K_{q1} + \dfrac{K_{i2}}{s}\right) - i_{rq}\right]\left(K_{p3} + \dfrac{K_{i3}}{s}\right) \\ \qquad - I_{sd} s\omega_s L_m - I_{rd} s\omega_s L_{rr} \end{cases}, \tag{19}$$

where: K_{p1}, K_{i1}, K_{p3}, K_{i3}, K_{q1}, K_{i2} are PI controller parameters in the rotor-side converter, ω_s is the rotational angular velocity of the synchronous magnetic field, and the d-q components in the stator-rotor currents are I_{sd}, I_{sq}, I_{rd}, I_{rq}, respectively. After adding PSS-VI, Eq. (19) can be written as

$$\begin{cases} V_{rd} = \left[\left(P_s^* - P_s\right)\left(K_{p1} + \dfrac{K_{i1}}{s}\right) - i_{rd}\right]\left(K_{p3} + \dfrac{K_{i3}}{s}\right) \\ \qquad - I_{sq} s\omega_s L_m - I_{rq} s\omega_s L_{rr} \\ V_{rq} = \left[\left(Q_s^* - Q_s\right)\left(K_{q1} + \dfrac{K_{i2}}{s}\right) - i_{rq}\right]\left(K_{p3} + \dfrac{K_{i3}}{s}\right) \\ \qquad - I_{sd} s\omega_s L_m - I_{rd} s\omega_s L_{rr} - u_{errs} \end{cases}, \tag{20}$$

where u_{errs} is the output signal of PSS-VI controller after AVR device.

$$u_{errs} = \frac{U_{\text{PSS-VI}} - \dfrac{u}{1 + sT_r}}{sT_e + K + \dfrac{sK_{f1}}{sT_{f1}} \dfrac{1 + sT_c}{1 + sT_b} \dfrac{K_a}{1 + sT_a}}, \tag{21}$$

where T_e, K_{f1}, T_c, T_b, T_{f1}, K_a, T_a and T_r are AVR parameters and u is the measured value from stator-side voltage.

The PSS signal regulates the rotor voltage phase angle, which is then input to the doubly-fed induction motor control module through coordinate transformation. The phase compensation link provides the necessary overrun characteristics to compensate for the lag phase. To prevent overshooting, the limiting link is primarily utilized to limit the PSS's adjustment to the rotor voltage phase angle.

3.2. Small disturbance stability analysis

According to Liapunov stability theory, the power system is first linearized, the state space equations of the system are derived, the corresponding eigenvalues are found, and the small disturbance stability of the power system is studied according to eigenvalue analysis.

The dynamic characteristics of the power system can be described by the differential-algebraic equation in Eq. (22):

$$\begin{cases} \dot{x} = f(\boldsymbol{x}, \boldsymbol{y}) \\ 0 = g(\boldsymbol{x}, \boldsymbol{y}) \end{cases}, \tag{22}$$

where $\boldsymbol{x}, \boldsymbol{y}$ are the state and output variables of the system respectively.

According to Lyapunov's first method, the Taylor series expansion of the system is performed at the stable point (x_0, y_0) and the linearized model is shown in Eq. (23):

$$\begin{bmatrix} \Delta\dot{x} \\ 0 \end{bmatrix} = \begin{bmatrix} \nabla_x f & \nabla_y f \\ \nabla_x g & \nabla_y g \end{bmatrix} \begin{bmatrix} \Delta\boldsymbol{x} \\ \Delta\boldsymbol{y} \end{bmatrix} = \begin{bmatrix} \boldsymbol{A}_1 & \boldsymbol{B}_1 \\ \boldsymbol{C}_1 & \boldsymbol{D}_1 \end{bmatrix} \begin{bmatrix} \Delta\boldsymbol{x} \\ \Delta\boldsymbol{y} \end{bmatrix}, \tag{23}$$

where $\nabla_x f = \partial f(xy)/\partial x$ denotes the gradient of function $f(xy)$ on x. Symbol $\nabla_y f$, $\nabla_x g$, $\nabla_y g$ has a similar meaning. Assume that $\nabla_x g$ is a non-singular matrix, Eq. (23) can be expressed as follows:

$$\Delta\dot{x} = [\boldsymbol{A}_1\boldsymbol{B}_1(\boldsymbol{D}_1)^{-1}\boldsymbol{C}_1]\Delta\boldsymbol{x} = \boldsymbol{A}\Delta\boldsymbol{x}, \tag{24}$$

where $\boldsymbol{A} = \boldsymbol{A}_1\boldsymbol{B}_1(\boldsymbol{D}_1)^{-1}\boldsymbol{C}_1$ is the system state matrix. Suppose the eigenvalues of matrix $\boldsymbol{A}$ are $\lambda_i = \alpha \pm j\beta$, $i = 1, \ldots, n$, which are n solutions of characteristic equation $\det(\boldsymbol{A} - \lambda\boldsymbol{I}) = 0$. The system oscillation frequency is $f = \beta/2\pi$, and the corresponding damping ratio is defined as:

$$\zeta\ (\%) = \frac{-\alpha}{\sqrt{\alpha^2 + \beta^2}} \times 100\%. \tag{25}$$

The right eigenvector $\boldsymbol{w}$ and the left eigenvector $\boldsymbol{v}$ are used to obtain the participation factors that reflect the relative contribution of the system state variables to the system model. $p_{ij} = \boldsymbol{w}_{ij}\boldsymbol{v}_{ij}/(\boldsymbol{w}_j^T\boldsymbol{v}_j)$ is denoted as the participation factor of the i-th state variable for the j-th eigenvalue. where, for any eigenvalue $\boldsymbol{\lambda}_i$, the n-dimensional column vector $\boldsymbol{w}_i$ that matches $\boldsymbol{A}\boldsymbol{w}_i = \lambda_i\boldsymbol{w}_i$ $(i = 1, 2, \ldots, n)$ is called the right eigenvector of $\boldsymbol{\lambda}_i$.The n-dimensional row vector $\boldsymbol{v}_i$ conforming to $\boldsymbol{v}_i\boldsymbol{A} = \boldsymbol{v}_i\lambda_i$ $(i = 1, 2, \ldots, n)$ is called the left eigenvector of $\boldsymbol{\lambda}_i$. In fact, the small disturbance stability analysis is carried out by solving for the eigenvalues of the matrix $\boldsymbol{A}$. If all eigenvalues have negative real parts, then the entire system is asymptotically stable. If at least one eigenvalue has a positive real part, then the whole system is unstable. If none of the eigenvalues have a positive real part but at least one is zero, then the entire system is critically stable.

4. Simulation analysis

In order to study the performance of the proposed method, a DFIG-PSS-VI model is created in DIGSilent/PowerFactory, and analyzed on a 4-machine, 2-area interconnected system using the characteristic root analysis and time-domain simulation of Sections 3.2 and 3.3. The reference capacity of the example system is 100 MVA, the frequency is 50 Hz, and the power transmitted by the tie-line is 400 MW. In this system, area 1 and area 2 are connected by means of a double busbar. The four thermal power units G1, G2, G3 and G4 have a rated capacity of 900 MVA. The bus voltage on the generator side is 20 KV. The reference node is node 3, and the active output of each generator set is 700 MW. The DFIG access point is bus 10, and the system diagram is shown in Fig. 6.

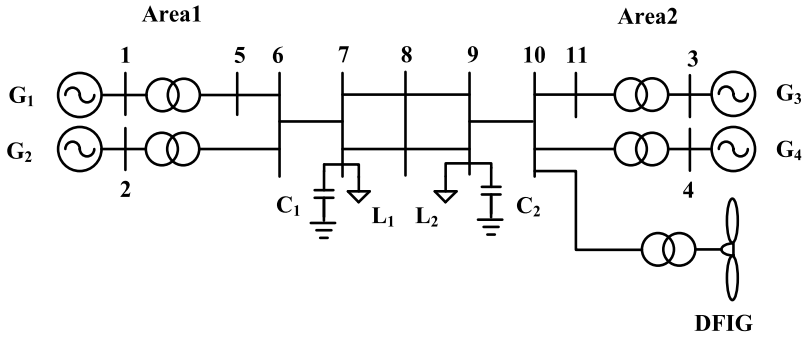

Fig. 6. The diagram of 4-machine 2-area system

4.1. Controller parameters influence analysis

The PSS-VI controller gain K_{PSS} is adjusted with the other control parameters unchanged, and according to Eq. (8), when K_{PSS} changes, the DFIG output voltage will change accordingly. The distribution of the characteristic root of oscillation mode 4 between system regions is shown in Fig. 7(a), which is related to all the generators. Where oscillation mode 4 indicates the new inter-regional oscillation between region 1 and 2 after DFIG access. The natural oscillation frequency suppression of electromechanical oscillation mode 4 is analyzed according to the variation of the real and imaginary parts of the characteristic roots, thus reflecting the influence of PSS-VI on the damping ratio of the system.

Based on Fig. 7(a), it can be observed that an increase in the PSS-VI gain KPSS results in a corresponding increase in the controller's additional damping. Furthermore, the oscillation mode 4 characteristic root within the system region tends to shift left and the damping ratio tends to increase.

Taking the PSS-VI controller gain $K_{\mathrm{PSS}} = 0.3$, keeping other parameters constant and changing the virtual impedance link parameter K_r. The distribution of the characteristic roots of the interregional oscillation mode 4 of the system is given in Fig. 7(b).

According to Fig. 7(b), it can be observed that as K_r increases, the real part of the eigenvalue for electromechanical oscillation mode 4 exhibits a slight rightward shift. As K_r decreases, the real part of this eigenvalue continues to move away from the imaginary axis and shows

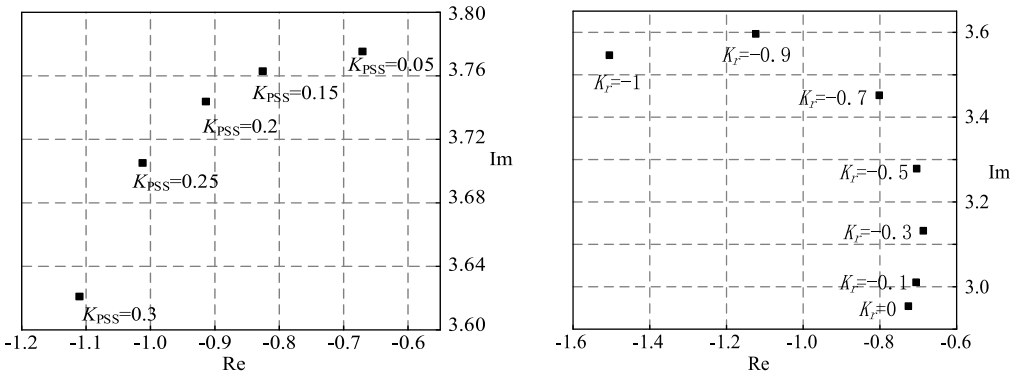

(a) Effect of K_{PSS} on characteristic roots (b) Effect of K_r on characteristic roots

Fig. 7. Effect of controller parameters on system characteristic roots

a clear tendency towards leftward movement on the complex plane. Meanwhile, its imaginary part gradually increases, indicating an increase in oscillation frequency.

When the gain K_{PSS} of PSS-VI is too small, the additional damping provided by the controller is relatively limited, resulting in a weak damping support effect on the system. Conversely, if K_{PSS} is set to an excessively large value, which will result in an excessively low oscillation frequency in electromechanical oscillation mode 4; if K_r is too large, it will cause the electromechanical oscillation mode 4 to oscillate at a high frequency. Therefore, considering the additional damping effect of the controller and the effect on the frequency of the oscillation mode, $K_{PSS} = 0.2$ and $K_r = -0.7$ are taken in this paper.

According to the previous analysis, take the PSS-VI parameters: $T_W = 0.01$, $T_1 = 0.08$, $T_2 = 0.4$, $T_3 = 0.3$, $T_4 = 0.06$, $K_{PSS} = 0.3$, $K_r = -1.2$, $K_l = 1.2$. Analyze the system's robustness under various working conditions.

4.2. Scenario I

Case a: 300 MW of power is delivered via the tie-line from area 2 to 1.

Case b: 400 MW of power is delivered via the tie-line from area 2 to 1. This is the basic operation mode.

Case c: 600 MW of power is delivered via the tie-line from area 2 to 1.

Table 1 indicates the variation of the eigenvalues, frequencies, and damping ratios of the system in different cases and modes. The damping ratio ζ is calculated by Eq. (25). Among them, modes 1 and 2 represent local oscillations in regions 1 and 2, modes 3 and 4 represent regional oscillations in regions 1 and 2.

To validate the performance of PSS-VI, assuming a 5% step change in active power of system load L1 at 1 s, followed by recovery at 1.5 s, with tie-line transmission of 400 MW and simulation time of 20 s. The curves of the relative power angle δ for G1 and the voltage change for bus 6 before and after the system addition of PSS-VI when load fluctuation occurs are presented in Fig. 8.

Table 1. Electro-mechanical oscillatory modes under different cases

Case	Mode	λ	f [Hz]	ζ [%]	Related unit
a	1	$-0.588 \pm j6.404$	1.019	9.154	G1, G2
	2	$-0.671 \pm j6.550$	1.043	10.195	G3, G4
	3	$-0.293 \pm j3.290$	0.524	8.879	G1–G4
	4	$-0.687 \pm j3.489$	0.555	19.319	G1–G4, DFIG
b	1	$-0.620 \pm j6.393$	1.018	9.658	G1, G2
	2	$-0.651 \pm j6.547$	1.042	9.897	G3, G4
	3	$-0.298 \pm j3.137$	0.499	9.464	G1–G4
	4	$-0.689 \pm j3.482$	0.554	19.417	G1–G4, DFIG
c	1	$-0.634 \pm j6.532$	1.040	9.666	G1, G2
	2	$-0.660 \pm j6.375$	1.015	10.291	G3, G4
	3	$-0.314 \pm j2.859$	0.455	10.942	G1–G4
	4	$-0.690 \pm j3.465$	0.551	19.536	G1–G4, DFIG

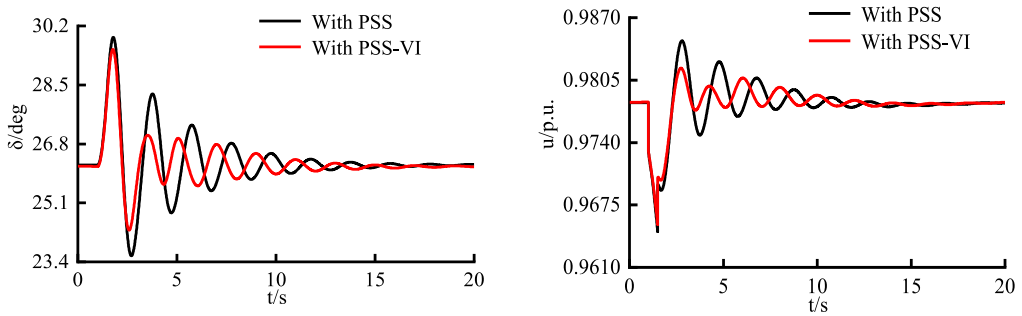

(a) The power angle for G1

(b) The voltage for bus 6

Fig. 8. System response curves for power angle and busbar under load fluctuation fault

According to Fig. 8, when the system is disturbed by the load fluctuation, the amplitude of the generator G1 relative to the power angle curve after the addition of PSS-VI is weaker in the first swing. The amplitude of the power angle is weakly reduced in the first swing, but the amplitude of the power angle curve is greatly suppressed after the second pendulum. For the bus 6 voltage, the amplitude of bus 6 voltage oscillation is effectively suppressed in the first swing when the system is disturbed. This effectively verifies that the addition of PSS-VI has a good suppression effect on the system oscillation and improves the DFIG. This effectively verifies that the addition of PSS-VI has a better suppression effect on the system oscillation and improves the damping characteristics of the system after the DFIG wind turbine is connected to the grid.

Assuming a three-phase short circuit occurs between tie-line 6 and 7 at $t = 1$ s, with the fault being cleared at $t = 1.1$ s and a simulation time of 20 s, Fig. 9 illustrates the relative power angle δ variation curves of generators G1 and G2.

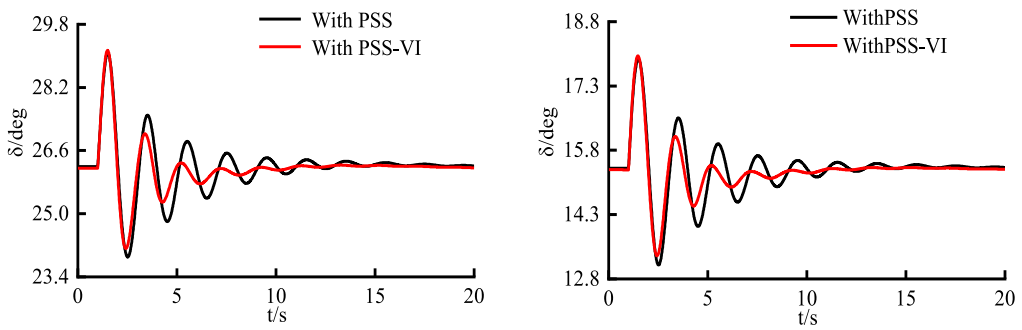

(a) The power angle for G1 (b) The power angle for G2

Fig. 9. Response curve of power angle der three-phase short-circuit fault of the system

According to Fig. 9, It can be that the second swing amplitudes of the power angle curves of both generators G1 and G2 are effectively suppressed when a three-phase short-circuit fault occurs in the system, and it can be seen that DFIG-PSS-VI still has a significant improvement effect on the system oscillation under different operating conditions and improves the damping characteristics of the system.

4.3. Scenario II

Case a: 300 MW of power is delivered via the tie-line from area 1 to 2.

Case b: 400 MW of power is delivered via the tie-line from area 2 to 1.

Case c: 600 MW of power is delivered via the tie-line from area 1 to 2.

According to Eq. (25), Table 2 is obtained, which indicates the degree of improvement of damping ratio for various oscillation modes under different operating conditions after DFIG is retrofitted with PSS and PSS-VI controllers, respectively. Based on the analysis presented in Table 2, it can be observed that the DFIG-PSS and DFIG-PSS-VI controllers do not exhibit a significant improvement or even show a slight reduction in damping ratios for intra-area oscillation mode 1 under different scenarios.

Furthermore, there is no noticeable left-shift trend in the corresponding eigenvalues, indicating that these controllers are less effective in enhancing damping ratios for intra-area oscillation mode 1. For intra-regional oscillation mode 2, DFIG-PSS and DFIG-PSS-VI have no significant improvement in the damping ratio for oscillation mode 2 under both case a and case b, and a small improvement in the damping ratio under case c. For the inter-area oscillation mode 3, the damping effect of DFIG-PSS-VI on the system is significantly better than that of DFIG-PSS as the transmission power of the tie-line increases, especially in case b, the damping ratio corresponding to the inter-area oscillation mode 3 is increased by 6.15% after the DFIG is attached with the PSS-VI controller, while there is a significant negative effect on the damping ratio after the PSS is

Table 2. Oscillation of the system containing PSS and PSS-VI in different case modes

Case	Mode	With PSS			With PSS-VI			Related unit
		λ	f [Hz]	ζ [%]	λ	f [Hz]	ζ [%]	
a	1	$-0.585 \pm j6.402$	1.019	9.101	$-0.580 \pm j6.400$	1.018	9.028	G1, G2
	2	$-0.671 \pm j6.550$	1.042	10.195	$-0.617 \pm j6.550$	1.043	10.196	G3, G4
	3	$-0.292 \pm j3.276$	0.521	8.888	$-0.282 \pm j3.295$	0.525	8.528	G1–G4
	4	$-0.605 \pm j2.928$	0.466	20.256	$-1.343 \pm j3.596$	0.572	34.992	G1–G4, DFIG
b	1	$-0.616 \pm j6.389$	1.017	9.601	$-0.614 \pm j6.389$	1.017	9.526	G1, G2
	2	$-0.651 \pm j6.547$	1.042	9.897	$-0.651 \pm j6.547$	1.042	9.597	G3, G4
	3	$-0.265 \pm j3.165$	0.504	8.331	$-0.318 \pm j3.156$	0.502	10.046	G1–G4
	4	$-0.619 \pm j2.907$	0.463	20.838	$-1.124 \pm j3.596$	0.572	29.822	G1–G4, DFIG
c	1	$-0.618 \pm j6.502$	1.035	9.466	$-0.618 \pm j6.502$	1.035	9.467	G1, G2
	2	$-0.699 \pm j6.348$	1.010	10.950	$-0.693 \pm j6.347$	1.010	10.851	G3, G4
	3	$-0.469 \pm j2.843$	0.452	16.279	$-0.403 \pm j2.359$	0.376	16.838	G1–G4
	4	$-0.512 \pm j2.444$	0.389	20.514	$-1.001 \pm j3.622$	0.576	26.646	G1–G4, DFIG

attached at the same position. For the inter-area oscillation mode 4, the DFIG additional PSS-VI controller improves the system damping ratio by 81.13%, 53.59%, and 36.39% for the three cases, which is significantly higher than the improvement with the additional PSS, but with the increase of the system tie-line power, the DFIG additional PSS-VI controller improves the system damping ratio for the inter-area oscillation mode 4. The improvement effect of DFIG with PSS-VI controller on the system damping ratio corresponding to inter-area oscillation mode 4 tends to decrease.

In order to more effectively verify the improvement effect of DFIG-PSS-VI on low frequency oscillation in the system, this paper assumes a 5% increase in active power for system load L1 at 1 s, with recovery occurring at 1.5 s and a simulation time of 20 s. Figure 10 and Fig. 11 show the power angle and voltage response curves when the system is subjected to load fluctuation and three-phase short circuit respectively under different cases.

From Fig. 10, it can be seen that the relative power angle δ of generator G1 and the amplitude of bus 6 voltage are significantly suppressed in the second swing when load fluctuations occur with the system under different tie-line power conditions, it shows that DFIG-PSS-VI has a significant improvement effect on the system robustness. From Fig. 11, it is evident that the relative power angle δ amplitude of generator G1 and G2 experience a significant reduction during a three-phase short-circuit fault in the system with varying tie-line transmission power. Additionally, the system restoration time is considerably shortened, indicating that DFIG-PSS-VI has a greater impact on enhancing system stability. By combining Fig. 10 and Fig. 11, it can be inferred that DFIG-PSS-VI significantly enhances system stability during load fluctuations, with the improvement effect gradually strengthening as the system tie-line power increases.

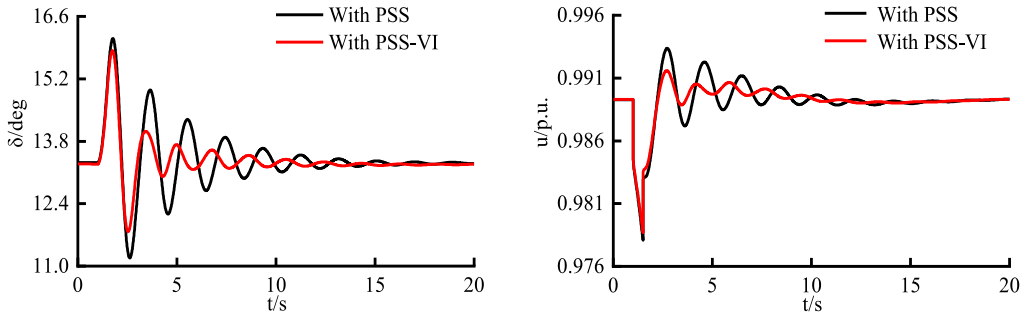

(a) The power angle for G1 in case a (b) The voltage for bus 6 in case a

Fig. 10. Response curve of power angle versus bus voltage under load fluctuation

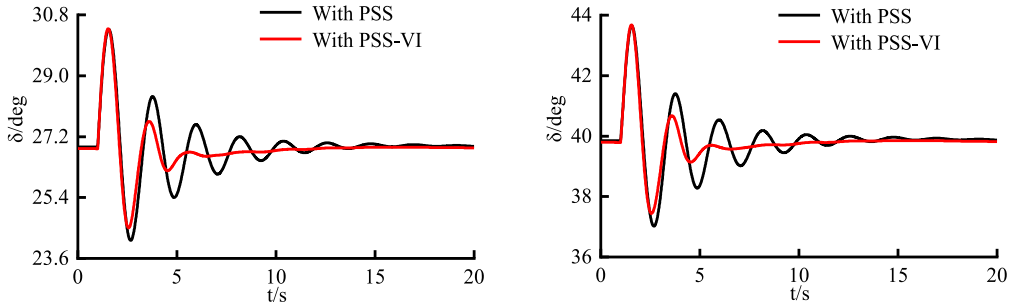

(a) The power angle for G1 in case c (b) The power angle for G2 in case c

Fig. 11. Response curve of power angle versus bus voltage under load fluctuation

5. Conclusion

For the low-frequency oscillation problem in the wind power grid-connected system, the paper designs the PSS-VI controller and verifies the enhancement effect of the virtual impedance link on the controller. The DFIG-PSS-VI model is designed and implemented in DigSILENT/PowerFactory. By taking the 4-machine,2-area system as an example, the constructed controller is added to the reactive power control loop of the doubly-fed wind turbine's rotor side controller. Finally, through time domain simulation, this paper demonstrate that the designed controller has effectively improved the low frequency oscillation characteristics of the system. In summary, the following conclusions can be drawn.

1. The proposed virtual impedance-based controller (PSS-VI) in this paper exhibits lower overshoot, superior robustness, and more significant improvement in system stability compared to the conventional controller (PSS).
2. After grid-connected wind power, the rotor-side reactive power control loop with PSS-VI in the DFIG can enhance the power system's low-frequency oscillation characteristics. It also has certain effects when the tie-line's power fluctuates.

3. The DFIG-PSS-VI controller with gain KPSS and virtual impedance has some effect on power system damping, which has limited effect on improving low-frequency oscillations within the region without wind power, but provides a new idea to suppress low-frequency oscillations between interconnected systems in the region containing wind power.

Acknowledgments

The authors gratefully acknowledge the research funding provided by the National Natural Science Foundation of China (NSFC) (No. 52377125), the Scientific and Technological Research Foundation of Henan Province (No. 222102320198), and the Key Project of Zhengzhou University of Light Industry (2020ZDPY0204).

References

[1] He P., Wen F.S., Xue Y.S., Gerard L., Wu D.Y., Lin Y., *Impacts of wind power integration on small signal stability and low frequency oscillation characteristics of interconnected power systems*, Dianli Xitong Zidonghua/Automation of Electric Power Systems, vol. 38, no. 22, pp. 1–10 (2014), DOI: 10.7500/AEPS20140613003.

[2] Wang Y., Meng J.H., Zhang X.Y., Xu L., *Control of PMSG-Based Wind Turbines for System Inertial Response and Power Oscillation Damping*, vol. 6, no. 2, pp. 565–574 (2015), DOI: 10.1109/TSTE.2015.2394363.

[3] Nie Y.H., Xu H.T., Cai G.W., Gao L., Zhao Y., Wu F.T., *Design of Wide-area Damping Controller Based on Immune System*, Dianwang Jishu/Power System Technology, vol. 44, no. 12, pp. 4713–4721 (2020), DOI: 10.13335/j.1000-3673.pst.2019.2703.

[4] Qi J., Wu Q., Chen K., Zhou D., Weng G.Q., *Additional Damping Control of Large Scale DFIG-based Wind Power Generation System Considering Time-varying Delays*, Dianwang Jishu/Power System Technology, vol. 43, no. 12, pp. 4440–4450 (2019), DOI: 10.13335/j.1000-3673.pst.2018.2925.

[5] He P., Wu X.X., Li C.S., Zheng M.M., Li Z., *Improvement of damping characteristics and index evaluation of a wind-PV-thermal-bundled power transmission system by combining PSS and SSSC*, Archives of Electrical Engineering, vol. 69, no. 3, pp. 705–721 (2020), DOI: 10.24425/aee.2020.133927.

[6] Zhu F., Zhao H.G., Liu Z.H., Kou H.Z., *The influence of large power grid interconnected on power system dynamic stability*, Zhongguo Dianji Gongcheng Xuebao/Proceedings of the Chinese Society of Electrical Engineering, vol. 27, no. 1, pp. 1–7 (2007), DOI: 0258-8013 (2007) 01-0001-07.

[7] Xue A., Wang J., Liu X., Li Y., *Survey and Prospect of Ultra-Low Frequency Oscillation Mechanism Analysis and Suppression in Power System*, Zhongguo Dianji Gongcheng Xuebao/Proceedings of the Chinese Society of Electrical Engineering, vol. 41, no. 2, pp. 553–567 (2021), DOI: 10.13334/j.0258-8013.pcsee.201191.

[8] Yu R., Jiang H., Ru H., Sun J., Liu B., Lai M., Tang F., *Mechanism and Damping Torque Analysis of Power System Stabilizer for Suppressing Ultra-low Frequency Oscillation*, 2nd IEEE China International Youth Conference on Electrical Engineering, CIYCEE 2021 (2021), DOI: 10.1109/CIYCEE53554.2021.9676764.

[9] Zhang Z., Wang H., Wang Z., Ding G., *Subsynchronous oscillation suppression measures for doubly-fed wind turbine based on eigenvalue analysis method and correlation factor method*, 6th International Conference on Systems and Informatics, ICSAI 2019, pp. 234–238 (2019), DOI: 10.1109/ICSAI48974.2019.9010200.

[10] He P., Wen F.S., Xue Y.S., Wang K.W., Gerard L., *Performance comparison of four kinds of power system stabilizers*, Dianli Xitong Zidonghua/Automation of Electric Power Systems, vol. 37, no. 3, pp. 30–37 (2013), DOI: 10.7500/AEPS201205232.

[11] Li Q.L., Wu C., Chen L., Duan R.H., Huang W., Min Y., *Parameter Optimization of Power System Stabilizer for Suppressing Frequency Oscillation*, Dianli Xitong Zidonghua/Automation of Electric Power Systems, vol. 44, no. 7, pp. 93–99 (2020), DOI: 10.7500/AEPS20190803005.

[12] Wu K.Y., Lu C.C., Wu L., Pu J., Huang X.M., *A new PSS with double-signal input and its simulation research*, Dianwang Jishu/Power System Technology, vol. 40, no. 5, pp. 1462–1468 (2016), DOI: 10.13335/j.1000-3673.pst.2016.05.025.

[13] Tummala A.S.L.V., *A robust composite wide area control of a DFIG wind energy system for damping inter-area oscillations*, Protection and Control of Modern Power Systems, vol. 5, no. 1 (2020), DOI: 10.1186/s41601-020-00170-y.

[14] Dominguez-Garcia J.L., Gomis-Bellmunt O., Bianchi F.D., Sumper A., *Power oscillation damping supported by wind power: A review*, Renewable and Sustainable Energy Reviews, vol. 16, no. 7, pp. 4994–5006 (2012), DOI: 10.1016/j.rser.2012.03.063.

[15] Liu Y., Gracia J.R., King T.J., Liu Y.L., *Frequency Regulation and Oscillation Damping Contributions of Variable-Speed Wind Generators in the U.S. Eastern Interconnection (EI)*, IEEE Transactions on Sustainable Energy, vol. 6, no. 3, pp. 951–958 (2015), DOI: 10.1109/TSTE.2014.2318591.

[16] Singh M., Allen A.J., Muljadi E., Gevorgian V., Zhang Y.C., Santoso S., *Interarea Oscillation Damping Controls for Wind Power Plants*, IEEE Transactions on Sustainable Energy, vol. 6, no. 3, pp. 967–975 (2015), DOI: 10.1109/TSTE.2014.2348491.

[17] Fan L.L., Yin H.P., Miao Z.X., *On active/reactive power modulation of DFIG-based wind generation for interarea oscillation damping*, IEEE Transactions on Energy Conversion, vol. 26, no. 2, pp. 513–521 (2011), DOI: 10.1109/TEC.2010.2089985.

[18] Johnson R.K., Klemm N.S., De Laneuville H., Koetschau S.G., Wild G., *Power modulation of Sidney HVDC scheme - I: RAS control concept, realization and field tests*, IEEE Transactions on Power Delivery, vol. 4, no. 4, pp. 2145–2152 (1989), DOI: 10.1109/61.35641.

[19] Wu X., Guan Y.J., Ning W., Jiang P., Xu Y., *Mechanism of Interactive Effect of RSC Parameters in DFIG on SSO and its Application*, Dianwang Jishu/Power System Technology, vol. 42, no. 8, pp. 2536–2543 (2018), DOI: 10.13335/j.1000-3673.pst.2017.2721.

[20] Shenghu L., Qi S., Xuemei S., Jiejie H., *Suppression of weakly damped low-frequency modes of wind power system based on regional pole placement*, Power System Protection and Control, vol. 45, no. 20, pp. 14–20 (2017), DOI: 10.7667/PSPC201704.

[21] Li S., Zhang H., *Sensitivity analysis of the oscillation modes to the transfer function of DFIG-PSS in a wind power system*, Dianli Xitong Baohu yu Kongzhi/Power System Protection and Control, vol. 48, no. 16, pp. 11–17 (2020), DOI: 10.19783/j.cnki.pspc.191235.

[22] Hughes F.M., Anaya-Lara O., Jenkins N., Strbac G., *A power system stabilizer for DFIG-based wind generation*, IEEE Transactions on Power Systems, vol. 21, no. 2, pp. 763–772 (2006), DOI: 10.1109/TPWRS.2006.873037.

[23] Zhou P., Zhang X.Y., Di Q., Yue J.H., Xing C., *Pre-synchronous Grid-connection Strategy of DFIG-based Wind Turbine with Virtual Synchronous Generator Control*, Dianli Xitong Zidonghua/Automation of Electric Power Systems, vol. 44, no. 14, pp. 71–78 (2020), DOI: 10.7500/AEPS20191224010.

[24] Ju Y.T., Ma Y.R., Qi Z.N., *Research on the Effect Mechanism of Virtual Synchronous Generator on Small-signal Stability Based on Damped Torque Analysis*, Zhongguo Dianji Gongcheng Xuebao/Proceedings of the Chinese Society of Electrical Engineering, vol. 40, pp. 98–107 (2020), DOI: 10.13334/j.0258-8013.pcsee.200129.

[25] Paszek S., Noco A., Pruski P., *The use of PSS2A system stabilisers to damp electromechanical swings in medium voltage networks with distributed energy sources*, Archives of Electrical Engineering, vol. 71, no. 3, pp. 717–719 (2022), DOI: 10.24425/aee.2022.141681.